Korean Journal of Remote Sensing, Vol.27, No.3, 2011, pp.259~276

Detection of short-term changes using MODIS daily dynamic cloud-free composite algorithm

Sun-Hwa Kim †, Jeong Eun, Sung-Jin Kang, and Kyu-Sung Lee

Inha University, Department of Geoinformatic Engineering

Abstract : Short-term land cover changes, such as forest fire scar and crop harvesting, can be detected by high temporal resolution satellite imagery like MODIS and AVHRR. Because these optical satellite images are often obscured by clouds, the static cloud-free composite methods (maximum NDVI, minblue, minVZA, etc.) has been used based on non-overlapping composite period (8-day, 16-day, or a month). Due to relatively long time lag between successive images, these methods are not suitable for observing short-term land cover changes in near-real time. In this study, we suggested a new dynamic cloud-free composite algorithm that uses cut-and-patch method of cloud-masked daily MODIS data using MOD35 products. Because this dynamic composite algorithm generates daily cloud-free MODIS images with the most recent information, it can be used to monitor short-term land cover changes in near-real time. The dynamic composite algorithm also provides information on the date of each pixel used in compositing, thereby makes accurately identify the date of short-term event.

Key Words : MODIS, short-term change, cloud-free, composite, dynamic

1. Introduction

Since the 1970s, Advanced Very High Resolution Radiometer(NOAA-AVHRR) and Moderate Resolution Imaging Spectroradiometer(MODIS) of the National Oceanic and Atmospheric Administration have been used to detect a short-term geophysical events of the earth surface, covering the entire Earth every 1 to 2 days. These high temporal resolution satellite images were used to detect short-term changes in land surface reflectance(Gao *et al.*, 2006; Hansen *et al.*, 2008; Potapov *et al.*, 2008; Hilker *et al.*, 2009). For example, MODIS thermal anomaly (MOD14) provides images of wild fires occurring over the world on a daily basis(Kaufman and Justice, 1998). However, cloud covered areas obscure the observations, thereby, seriously inhibit the abilities of AVHRR or MODIS to monitor short-term changes occurring at the land surface(Cihlar *et al.*, 2004; Julien and Sobribno, 2010). A static cloud-free composite method developed to alleviate the cloud cover entails selecting pixels with the highest quality from multiple scenes within a predefined time interval and merging them into a composite image..

Received May 19, 2011; Revised June 17, 2011; Accepted June 18, 2011.

† Corresponding Author: Sun-Hwa Kim (rs_sun@inha.ac.kr)

The method consists of periods spanning 8 days, 16 days or one month. The cloud-free composite method also reduces atmospheric constituents(Breaker *et al.*, 2010; Cihlar, 1996; Eidenshink and Faundeen, 1994; Fontana *et al.*, 2009; Holben, 1986; Robertson *et al.*, 1992; Saleous *et al.*, 2000). Image composition entails selecting pixels with the highest quality from multiple scenes within a predefined time interval and merging them into a composite image(Fontana *et al.*, 2009). A static cloud-free composite method has been widely used to monitor vegetation(Botta *et al.*, 2000; Dickinson *et al.*, 1986; Potter *et al.*, 2003; Tian *et al.*, 2004; Yang *et al.*, 2006), land surface phenology(de Beurs and Henebry, 2004; White and Nemani, 2006), burned land area(Chuvieco *et al.*, 2008; Fernandez *et al.*, 1997; Stroppiana *et al.*, 2002), and land cover mapping and land cover changes around the world(Bonan *et al.*, 2003; de Beurs and Henebry, 2004; Latifivic *et al.*, 2004).

Several AVHRR cloud-free composite products are currently available: seven-day and monthly composite global vegetation index(GVI) and Global Inventory and Monitoring and Modelling Study(GIMMS) AVHRR 8km resolution of normalized difference vegetation index(NDVI) 15-day composite data set(Fontana *et al.*, 2009; Pinzon *et al.*, 2005; Tucker *et al.*, 2005). Using MODIS observation, several composite products including 1km NDVI 16-day composite(MOD13A2, collection 5), 8-day composite snow cover(MOD10A2), 8-day composite leaf area index(MOD15A2), and 16-day composite albedo are available(MOD43)(Fensholt *et al.*, 2009; Hall *et al.*, 2002; Myneni *et al.*, 2002; Stroeve *et al.*, 2005; Yang *et al.*, 2006). The MODIS NDVI composite algorithm uses a maximum NDVI value with a constrained-view angle per composite interval(Gallo *et al.*, 2005). A 10-day SPOT/VEGETATION(VGT)-S product is a full resolution (1km resolution) providing a 10-day maximum value NDVI composite(Duchemin *et al.*, 2002; Holben, 1986; Latifovic *et al.*, 2004; Stroppiana *et al.*, 2002). Although these cloud-free NDVI composites from AVHRR, MODIS, and SPOT VEGETATION have been useful in time-series analysis, these products still include noise originated from residual clouds and calculating composite data(Asner *et al.*, 1998; Chen *et al.*, 2004; Cihlar and Howarth, 1994; Cilhar *et al.*, 1994; Duchemin *et al.*, 1999; Gutman, 1991; Gutman and Ignatov, 1995; Hall *et al.*, 1995; Holben, 1986; Li *et al.*, 1996). The radiometric calibration or viewing angle correction must be further made(Cihlar *et al.*, 1997; 2004; Duchemin *et al.*, 2002; Latifovic *et al.*, 2004).

The static composition algorithm comprises 8-day, 16-day, and a month periods. However, its low temporal resolution inhibits to detect events in land cover shorter than a week(Ahl *et al.*, 2006; Chuine *et al.*, 2000; Yang *et al.*, 2006). Because the static composite algorithm selects unburned pixels showing a higher NDVI value instead of burned pixels if the forest fire occur during the composite period(Chuvieco *et al.*, 2005). The static cloud-free composite algorithm may not appropriately in case of forest fire. In case of forest disturbance, 16-day composited NDVI less sensitive to forest disturbances than a single day MODIS NDVI because the highest NDVI value is selected over 16-day period(Jin and Sader, 2005). Therefore, a new composite algorithm is necessary for providing the most recent and more accurate information. The purpose of the study is to develop a new composite algorithm of MODIS data, which provides the most up to date information. The daily cloud-free composite would be very valuable to monitor short-term changes such as forest fires, forest disturbances, and crop harvesting.

2. Daily dynamic cloud-free composite algorithm

1) Dataset used

The Terra MODIS radiance data set consisting of 250 m and 500 m MODIS datasets(MOD02QKM, MOD02HKM) was used for fusion and the composite (Table 1). MODIS geolocation dataset(MOD03) was also used for re-projecting the MOD02 data*set al*ong with MOD35 product to retrieve cloud shadow and mask data. MODIS datasets exhibiting rainy, non-rainy and dry season conditions were retrieved in order to test and validate the daily dynamic composite algorithm. Cloud covered over 75% and under 40% during rainy and non-rainy seasons, respectively. Forest fires have occurred frequently in May with is most non-rainy month of a year in the Korean Peninsula. This composite algorithm was validated with the October 2009 and May 2010 dataset including forest fires and harvesting agricultural crops.

2) Pre-processing of MODIS dataset

MODIS radiance product(MOD02) data is the swath width product so that the geometric distortion of this dataset is less lower than sinusoidal projection tile product as MOD09 product(Luo *et al.*, 2008). The swath product was re-projected to the UTM coordinate system using the MRT-SWATH tool(https://lpdaac.usgs.gov/lpdaac/tools/modis_reprojection_tool_swath) and MODIS geolocation data(MOD03). The geometric accuracy of the re-projected MOD02 product was less than one pixel (http://www.ga.gov.au). After the preprocessing,

3) Generating of 250 m fusion images

The MODIS has a total of 36 spectral bands composed of two 250 m spatial resolution bands, five 500 m bands, and twenty nine 1km bands(Kim,

Table 1. Description of data set used for cloud-free composition

Items	Specifics	Notes
Product	MOD02QKM	250 m MODIS radiance data(2 bands)
		- Band 1: 620 ~ 670nm
		- Band 2: 841 ~ 876nm
	MOD02HKM	500 m MODIS radiance data(5 bands)
		- Band 1: 459 ~ 479nm
		- Band 2: 545 ~ 565nm
		- Band 3: 1,230 ~ 1,250nm
		- Band4: 1,628 ~ 1,652nm
		- Band5: 2,105 ~ 2,155nm
	MOD03	1 km MODIS Geolocation data
		- Solar azimuth/zenith angle
		- Sensor azimuth/zenith angle
		- Usage for re-projection of MOD02 data
	MOD35	1 km MODIS Cloud mask data
		- Usage for cloud and shadow detecting of MOD02 data
Date	July 1 ~ 31, 2009	Usage for compositing dataset acquired during rainy season
	October 1 ~ 31, 2009	Usage for compositing dataset acquired during clear-sky season and detecting the harvested paddy
	May 1 ~16, 2010	Usage for detecting the burned area

Table 2. Correlation between bands of Terra MODIS data

Bands	Band1	Band2	Band3	Band4	Band5	Band6	Band7
Band 1(Red)	1.000	-	-	-	-	-	-
Band 2(NIR)	0.635	1.000	-	-	-	-	-
Band 3(Blue)	**0.577**	-0.050	1.000	-	-	-	-
Band 4(Green)	**0.502**	0.238	0.876	1.000	-	-	-
Band 5(NIR)	0.465	**0.927**	-0.174	0.141	1.000	-	-
Band 6(SWIR)	0.556	**0.910**	0.088	0.249	0.973	1.000	-
Band 7(SWIR)	0.637	**0.875**	0.014	0.361	0.930	0.981	1.000

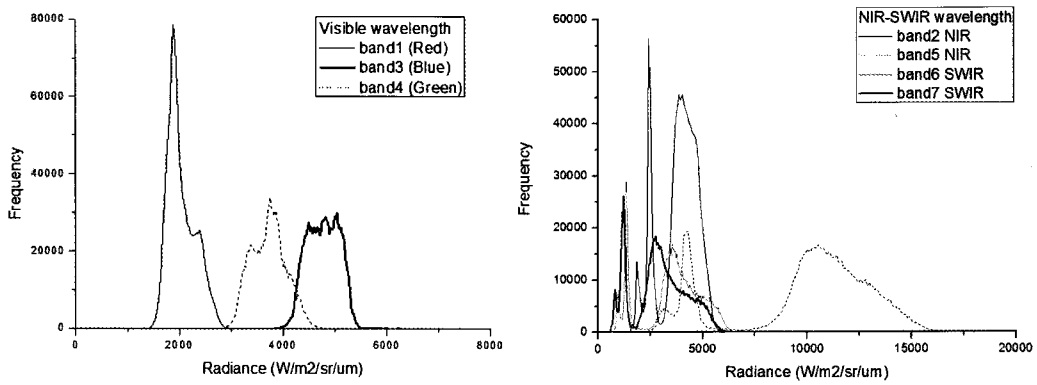

Fig. 1. Histograms of MOD02 visible and infrared wavelength.

2003). However, some limitations existed when using 500 m or the 1km spatial resolution MODIS data within small areas including complex land cover types(Jepsen *et al.*, 2009; Kim and Lee, 2003). Thus, seven 250 m spatial resolution MODIS bands were newly generated by fusing two MODIS 250 bands into five 500 m bands using local mean and variance matching(LMVM) fusion method(Kim *et al.*, 2010; Eq.1). In order to achieve the best band combination, we analyzed the statistics and histogram of the MODIS bands, as shown in Table 2 and Fig. 1. Band 1(red) exhibited higher correlations with band 3(blue), and band 4(green), and band 2(NIR) were correlated to band 4(NIR), band 5(NIR), band 6(SWIR) and band 7(SWIR). In Fig. 1, the histograms of bands 1, 3, 4 show uni-modal distributions and bands 2, 5, 6, 7 show the tri-modal distribution in its frequency versus radiance(Fig. 1). Using the spectral similarity between bands, the 250 m band 1(red) and 500 m band 3(blue), 4(green) were fused, and 250 m band 2(NIR) and 500 m MODIS band 5(NIR), 6(SWIR), 7(SWIR) were fused.

Among various fusion methods, the local mean and variance matching(LMVM) fusion method showed the best MODIS fusion results in regards to spatial resolution and spectral fidelity(Kim *et al.*, 2010). The LMVM filter shown in Formula 1 was applied to normalize the high resolution and low resolution image using the local mean and variance value of the two target images. Using local statistics of high and low resolution image, the correlation between the fused image and low resolution image increased more than other fusion methods (Karathanassi *et al.*, 2007).

$$F_{i,j} = \frac{(HR_{i,j} - \overline{HR_{i,j(w,h)}} \times std*(LR)_{i,j(w,h)})}{std(HR)_{i,j(w,h)}} + \overline{LR_{i,j(w,h)}} \quad (1)$$

$F_{i,j}$: MODIS 250 m fused image at pixel coordinates i, j

$H_{i,j}$: MODIS 250 m original image at pixel coordinates i, j

$\overline{LR_{i,j(w,h)}}$: The local mean of MODIS 500 m original image calculated inside the window of size (w, h) at pixel coordinates i, j

$\overline{HR_{i,j(w,h)}}$: The local mean of MODIS 250 m original image calculated inside the window of size (w, h) at pixel coordinates i, j

$std(LR)_{i,j(w,h)}$: The local standard deviation of MODIS 500 m original image calculated inside the window of size(w, h) at pixel coordinates i, j

$std(HR)_{i,j(w,h)}$: The local standard deviation of MODIS 250 m original image calculated inside the window of size(w, h) at pixel coordinates i, j

4) Cloud and shadow detection method

The proposed daily dynamic composite algorithm used the cut and patch method on the cloud area of each MODIS image. Thus, the accuracy of cloud and shadow detection is of paramount importance. Visible or thermal wavelength bands were used earlier for detecting the cloud(Ackerman *et al.*, 2006; Luo *et al.*, 2008). Thermal bands were found to be more accurate than visible bands for detecting cloud(Ackerman *et al.*, 2006; Chuvieco *et al.*, 2005). We used a MOD35 1km to detect cloud and shadow mask. Although the MOD35 cloud mask algorithm endured many threshold tests for different cloud types over the ocean, vegetation surfaces and desert surfaces(Ackerman *et al.*, 2006). In the cloud shadow detection algorithm, the geometric relationship between cloud location was determined as well as the solar and sensor location and angle(Ackerman *et al.*, 2006; Le Hégarat-Mascle and André, 2009; Simpson and Stitt, 1998). Applying the geometric detection algorithm to each cloud pixel requires extensive computing time(Ackerman *et al.*, 2006). The MOD35 shadow mask algorithm used the threshold test using reflectance bands(Ackerman *et al.*, 2006). Because MOD35 algorithm is insensitive to detect thin clouds on the cloud boundary, clouds are still shown on the cloud edge in the MODIS image masked. For more accurate masking of cloud and shadow, we applied the 250 m buffering at MOD35 cloud and shadow mask.

5) Daily dynamic cloud-free composite algorithm

Fig. 2 compares the static and daily dynamic cloud-free composite algorithm using MODIS data. The static composite algorithm produced one cloud-free image by compositing daily MODIS data during the static period(8-, 10-, 16- days, and a month). The proposed daily dynamic composite algorithm used multi-temporal MODIS data sets during the dynamic period, and produced daily cloud-free composite images. The optimal period of compositing was conducted by the cloud containments and multi-temporal MODIS data sets acquired at previous days were used for dynamic daily compositing, as shown in Fig. 2.

A procedure for generating daily dynamic cloud-free composite images is summarized in Fig.3. By fusing the 500 m MOD02HKM product and the 250

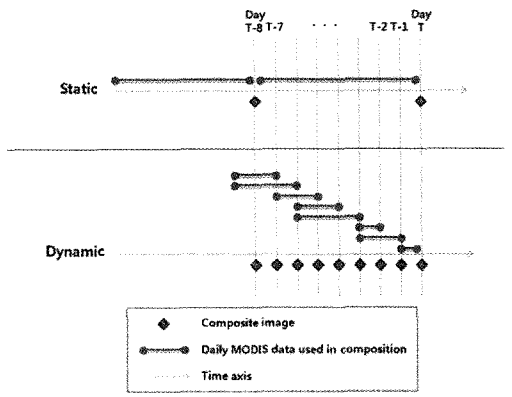

Fig. 2. A schematic diagram of temporal coverage in the static composite algorithm and proposed daily dynamic algorithm

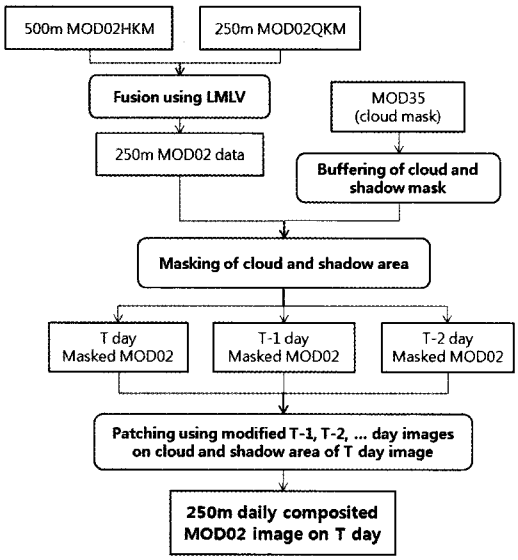

Fig. 3. A flow-chart of applying dynamic daily composite algorithm to MODIS data to obtain daily cloud-free land cover images with 250 m spatial resolution.

m MOD02QKM product, 250 m fused MODIS radiance images were generated. The daily dynamic cloud-free composite algorithm used the cut and patch method on the cloud area for the daily MOD02 dataset. The daily MOD02 dataset using cloud and shadow mask were used for dynamic cloud-free compositions. The cut area of MOD02 data on reference day T was patched by using other MOD02 dataset acquired at T-1, T-2 day, and so forth. The number of images used for the composition was determined by the amount of cloud cover of less than 5%. The number of images(days) is defined as the dynamic period. The static composite algorithm produces one cloud-free image by compositing daily MODIS data obtained during the static period(8-,10-,16- days, and a month). The proposed daily dynamic composite algorithm uses multi-temporal MODIS data during the dynamic period and produces daily cloud-free composite images(Fig.2).

6) Validation of daily dynamic cloud-free composite algorithm

In order to validate the proposed daily dynamic cloud-free composite algorithms, two events were chosen. A forest fire that occurred on 7 May, 2010 and its burned area was about 86 ha(National Forest Fire Information System, http://sanfire.forest.go.kr). With the information provided by the National Forest Fire Information system in combination with a google image, the boundary of the burned area was defined using the normalized burned ratio(NBR) was used. The NBR spectral index focused on mapping the burned area and assessing burn severity(Key and Benson, 1999; Loboda *et al.*, 2007). The spectral reflectance of the burned area increased in the SWIR and deceased in the NIR wavelength regions. The NBR index used this spectral difference of forest and burned area(Loboda *et al.*, 2007). The change of NBR value of composite images before and after forest fire was generated and analyzed.

$$NBR = \frac{\rho NiR(band2) - \rho SWIR(band7)}{\rho NiR(band2) + \rho SWIR(band7)} \quad (2)$$

Table 3. Information on the two study sites in South Korea

Site 1 : Forest fire		Site 2 : agricultural crop harvesting area	
Date of firing	May 7, 2010 12:56 ~ 19:10	Date of harvesting	October 19, 2009
Area	86 ha	Area	475 ha
Location	UTM 485,726.59E, 981,436.85 Mt. Bonghwa, Yeongcheonsi, Gyeongbukdo	Location	UTM 276865.2512E, 3854944.5074N Nearing Yeoungsan River, Jeollanamdo
Cause	Arson	Land use	Rice paddy

As additional short-term change, the harvest area is detected using compositing algorithm in this study. To detect the harvest area, two cloud-free NDVI datasets were generated using daily and 8-day composite images during October 2009. The NDVI and NDVI temporal patterns were analyzed at a rice paddy and then decreased after harvesting. Considering the geometric accuracy of MODIS data, relative relatively large rice paddy was selected. Table 3 shows detailed information about the site.

3. Results and discussion

1) Temporal and spatial distribution of cloud-free days over the Korean Peninsula

Due to the influence of East-Asian monsoon climate, Korean Peninsula may be climatologically characterized as cloudy summer and clear winter with a large temporal and spatial variability. For example, cloud-free days over the entire Peninsula were less than 3-4 days in July 2009, during summer and more than 20 days in October(Fig. 4). Therefore, the daily dynamic composite algorithm using MODIS data would generate only one or two cloud-free images in cloudy July, however, more than 20 images in clear October 2009. Fortunately, important events(e.g., forest fire and agricultural crop harvesting) occur in the land cover during the relatively cloud free periods in Korea.

The primary purpose generating both static and dynamic composites was to reduce the cloud containments and generate the cloud-free image. As shown in Fig. 4, the original daily MOD02 data showed higher cloud coverage especially during the rainy season. During the dynamic composite process, the cloud area was cut using MOD35 cloud and shadow mask and patched the cloudless area of other days. During the non-rainy season, the composited image under 10% cloud coverage was generated using three or four MOD02 daily images, however, composite image of less than 40% of cloud cover could be obtained(Fig.4). Generating the 100% cloud-free composited image would not be achievable even in September 2009(Fig. 4).

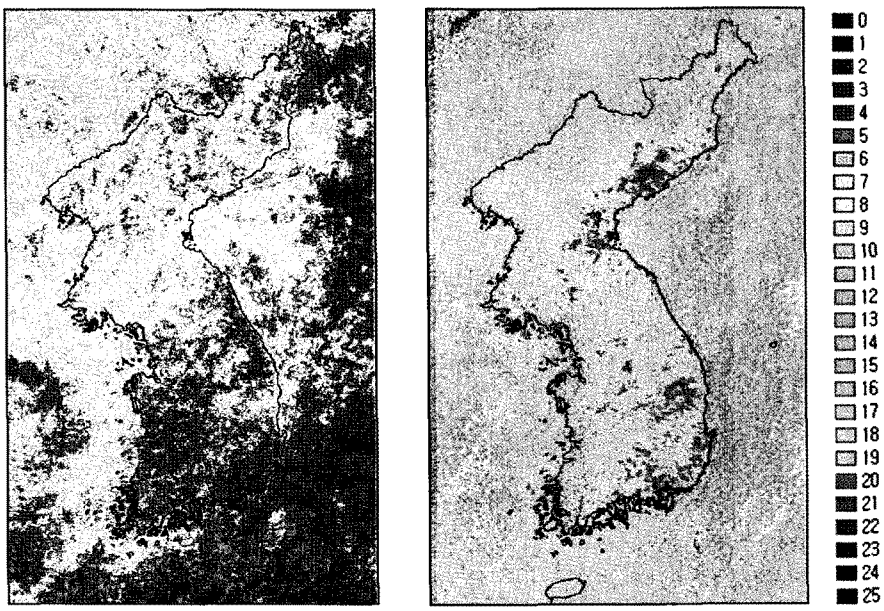

Fig. 4. Distribution of cloud-free days during July(left) and October 2009(right) over the Korean Peninsula

2) Effectiveness of daily dynamic cloud-free composite algorithm in dry season and wet season

An exemplary case of application of daily dynamic cloud-free composite algorithm is given here to illustrate its usefulness. The original MODIS image showed a small amount of clouds on 5 October 2009(Fig. 5a). A cloud-free image under 10% cloud cover can be generated using only two and three daily MODIS images in Fig. 5b and 5c, respectively using a cut and patch technique. Daily dynamic composite images provided date information of the MODIS images used in generating daily cloud-free composite images(Fig. 5e). Date information at each pixel of composite image helped to accurately detect short-term changes. The 8-day composite images generated by applying a minblue algorithm at eight MODIS images obtained during October 1~8 was also presented here as comparison.

During October in 2009, each daily dynamic composite was generated using two to six daily images(Table 4). The daily dynamic composite of October 11 and the cloud-free MODIS image were generated using only two daily MODIS images. The

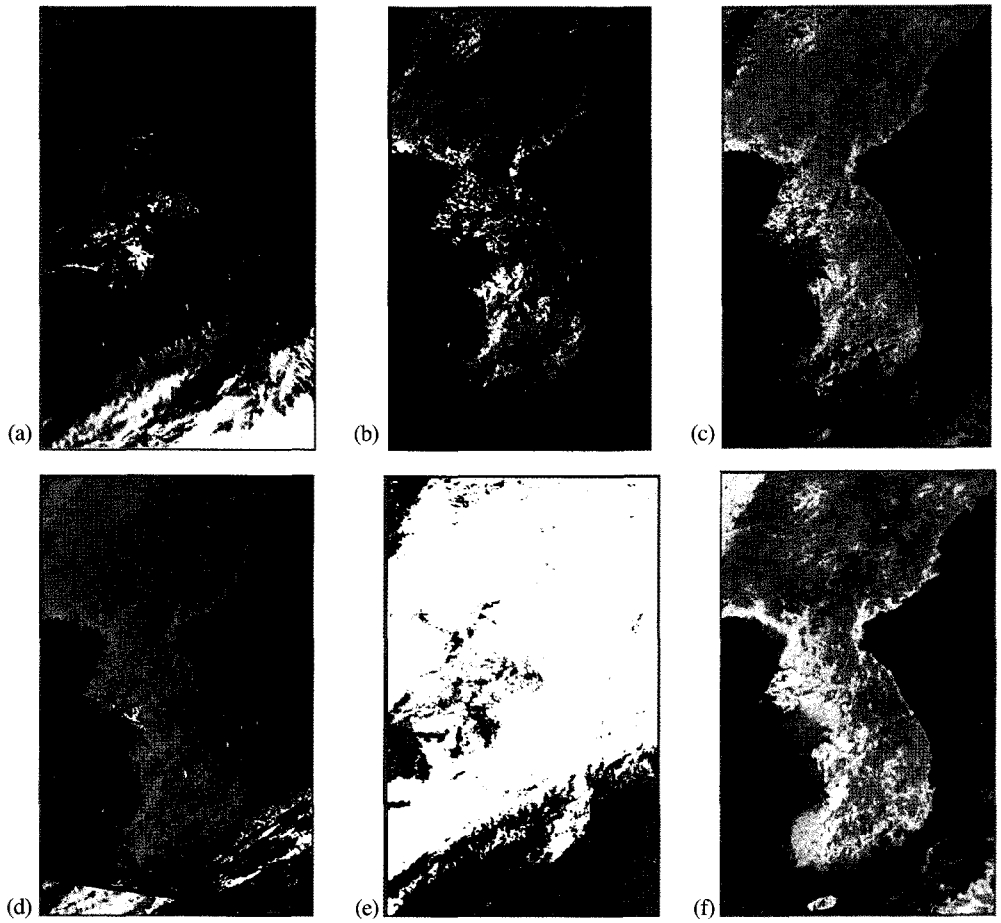

Fig. 5. (a) Original MODIS 250 m image,(b) MODIS image cut by the cloud and shadow obtained at October 5, 2009,(c) MODIS image composited using two MODIS daily images of October 5 and 4,(d) MODIS image composited using three MODIS daily images of October 5, 4, and 3,(e) date information of MODIS daily images used in dynamic compositing(white: October 5, gray: October 4, black: October 3),(f) 8-day composite image using ten images during October 1 ~ 8 day.

Table 4. Daily MODIS images used for the dynamic cloud-free composition during October 2009

Daily composite	MODIS images used	Daily composite	MODIS image used
October 3	October 3, 2, 1	October 18	October 18, 17, 15
October 4	October 4, 3, 2	October 19	October 19, 18, 17, 15
October 5	October 5, 4, 3	October 20	October 20, 19, 18
October 6	October 6, 5, 4	October 21	October 21, 20, 19, 18
October 8	October 8, 6, 5	October 22	October 22, 21, 20, 19
October 10	October 10, 8, 6	October 24	October 24, 22, 21, 20
October 11	October 11, 10	October 26	October 26, 24, 22, 21
October 12	October 12, 11, 10	October 27	October27, 26, 24, 22, 21
October 13	October 13, 12, 11, 10	October 28	October 28, 27, 26, 24
October 14	October14, 13, 12, 11, 10	October 29	October29, 28, 27, 26, 24
October 15	October 15, 14, 13	October 31	October 31, 29, 28, 27, 26, 24
October 17	October 17, 15, 14, 13		

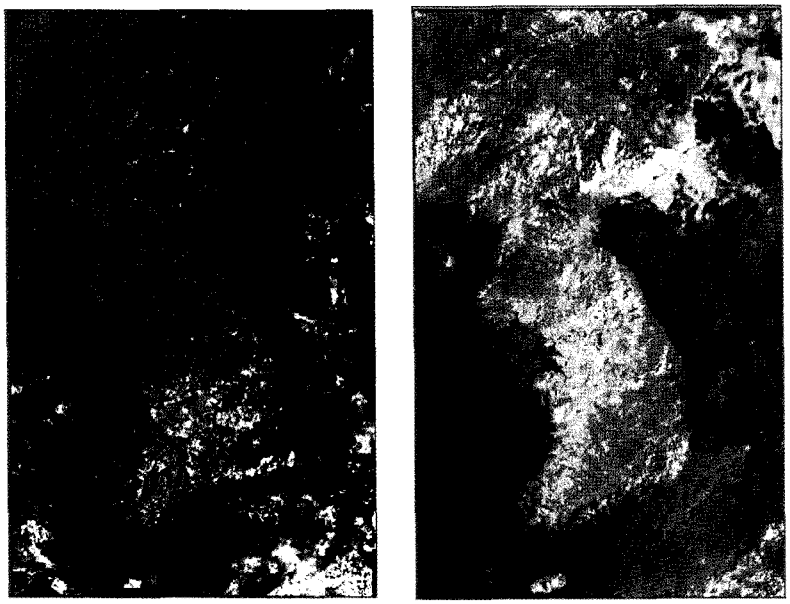

Fig. 6. Daily dynamic composite image(left) generated using 25 daily MODIS images from July 7 to 30, 2009 and 8-day composite image(right) generated using July 1~8 days

daily dynamic composition algorithm more effectively showed current information in contrast to the static composition algorithm during the non-rainy season.

In rainy season of July 2009, daily dynamic cloud-free composite algorithm allowed to composite 25 daily MODIS images(Fig. 6-left) opposed to the 8 day composite using a static composite algorithm(Fig. 6-right). The dynamic composite algorithm sacrificed the temporal resolution but enhanced spatial coverage, although both the two images still are not free from clouds.

3) Detection of short-term change in the land cover

The 8-day static composite algorithm uses the most pixels on a clear-sky day during the 8-day period while the daily cloud-free dynamic composite algorithm uses the most pixels on the latest day for

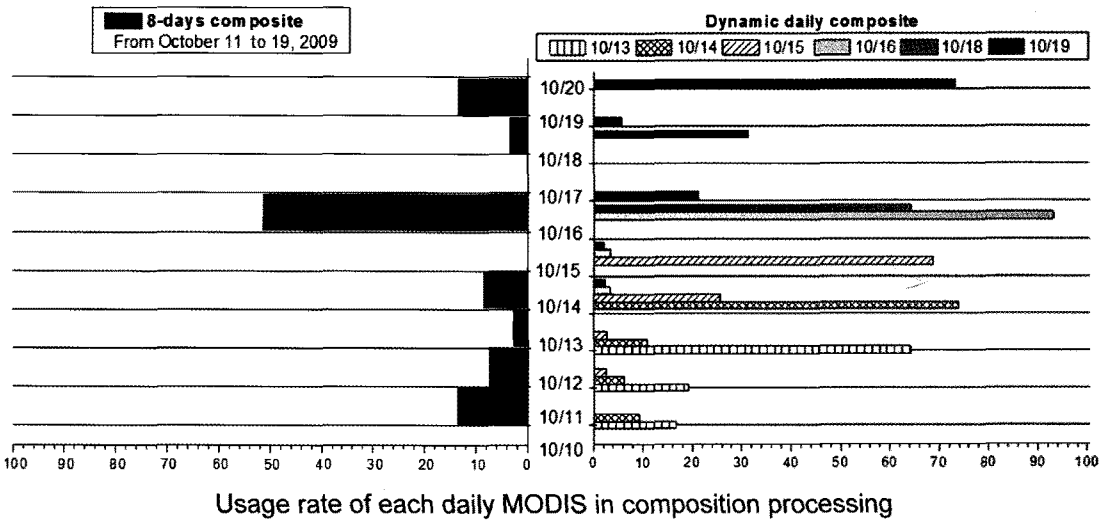

Fig. 7. Usage rate of daily MOD02 images(October 11~19, 2009, y axis) for 8-day composition and dynamic daily composition

each daily composition(Fig. 7). Therefore, the latest information is avail on the images generated using daily dynamic cloud-free composite algorithm and is useful to detect rapid changes, such as land cover events of forest fires or cultivations.

A forest fire occurred on 7 May 2010 in Mt. Bonghwa, Yeongcheon, Gyeonsangbukdo and some 80 ha of the area was burned(Table 3). In order to detect a burned area, daily 250 m cloud-free composite images on May 7 and 9 were generated (Fig. 8b and 8c, respectively). The 250 m fused daily composite image was sharper than the 500 m original MODIS color composite image(Fig. 8(a)) and the 500 m 8-day composited image(Fig. 8(d)). The LMVM fusion method provided the best fusion results for the spatial resolution and spectral fidelity. Fig. 8(b) is the cloud-free composite image of May 7 and Fig. 8(c) is the cloud-free composite of May 9 generated by three images during May 9, 8, and 7. The forest scar was detected in the daily dynamic cloud-free composite image obtained on May 9, 2 days after the fire. However, the 8-day composite image of May 1 to 8 obtained on May 8 did not show the burned area(Fig. 8(d)) but was detected on May 16 after 8 days from the date of the forest fire(Fig. 8(e)).

In order to detect the location of the forest fire scar, NBR images from dynamic and static composite data were generated. In the burned area, the NBR value decreased in comparison to the value prior to the forest fire(Fig. 9). After the forest occurred on 7 May, 2010, the NBR value decreased greatly. The burned area becomes visible on the dynamic cloud-free image on May 9 due to the heavy cloud on May 8. However, the burned area was detected much later on May 16 in 8-day composite data. As shown in Fig. 9, the dynamic composite algorithm provided short-time change information efficiently. The date from the dynamic composite product also accurately detected the dates on which short-term changes occurred. Because the 8-day composite image did not provide this date information, defining an accurate date on which short term changes occurred was difficult.

Fig. 10 shows short-term changes incurred from harvesting within a rice-paddy area(total 475ha) during October 19, 2010. In order to detect

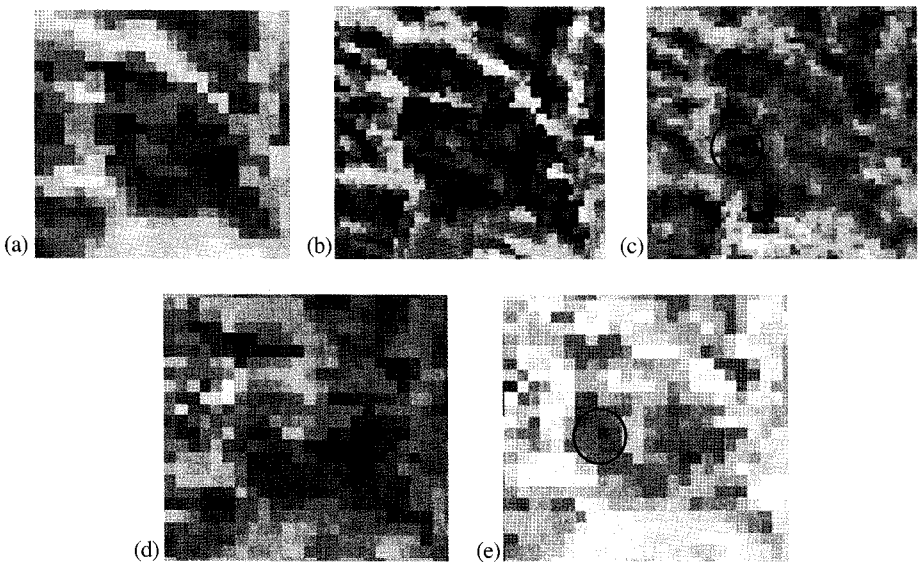

Fig. 8. Original 500 m MODIS color image of May 7, 2010(a), NIR-red-green color images of dynamic cloud-free composite images of May 7(b), May 9(c) and 8-day composite images during May 1~8(d) and 9-16 day(e)(black circle: burned area).

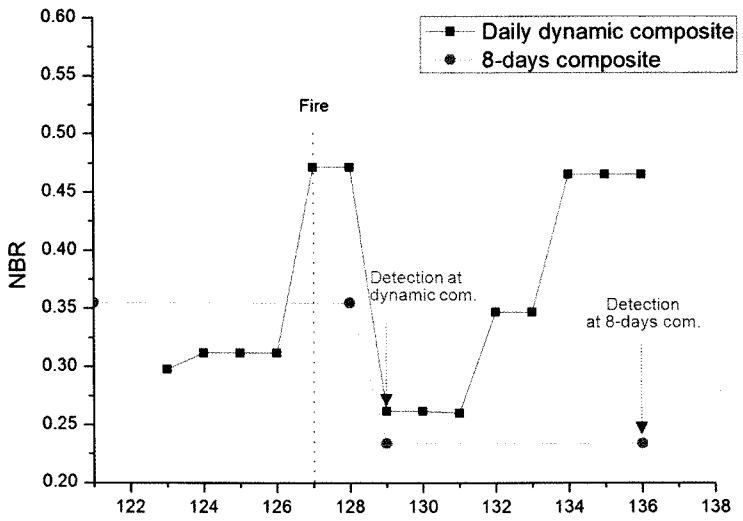

Fig. 9. NBR temporal pattern of dynamic composite and 8-day composite dataset at burned area.

harvesting, NDVI images using daily composite MODIS images of October 19 and 20 were generated(Fig. 10(a), (b)). In comparison to the 8-day composite NDVI images(Fig. 10(d)), the daily dynamic composite NDVI image showed the harvested area immediately after the change occurred(Fig. 10(b)).

Fig. 11 shows the NDVI temporal pattern of the dynamic composite images and the 8-day composite images in the harvested area during October 2009. The harvesting was detected in the dynamic composite image of October 19, 2009; at the harvesting was shown in the 8-day composite image during October 24-31, 2009. As shown in Fig. 11, the dynamic composite algorithm detected the harvest area and accurately defined the date of harvesting.

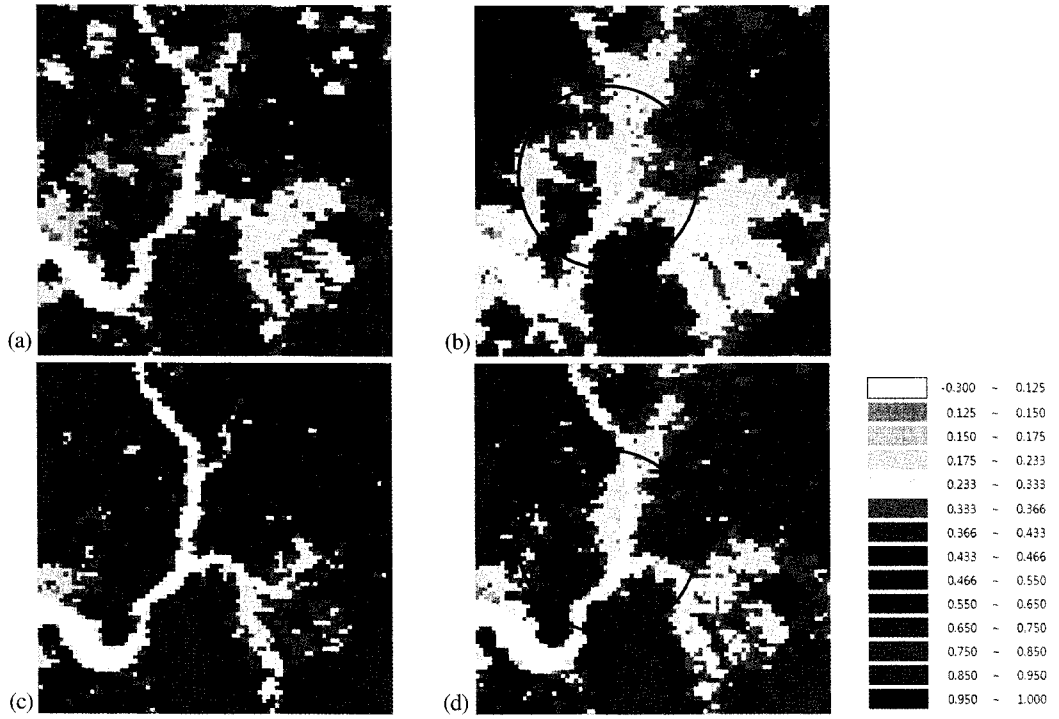

Fig. 10. Daily dynamic composite NDVI image of October 19(a), October 20(b), 8-day composite NDVI image during October 8 ~ 15(c), 16~23(d), and harvest area(black circle)

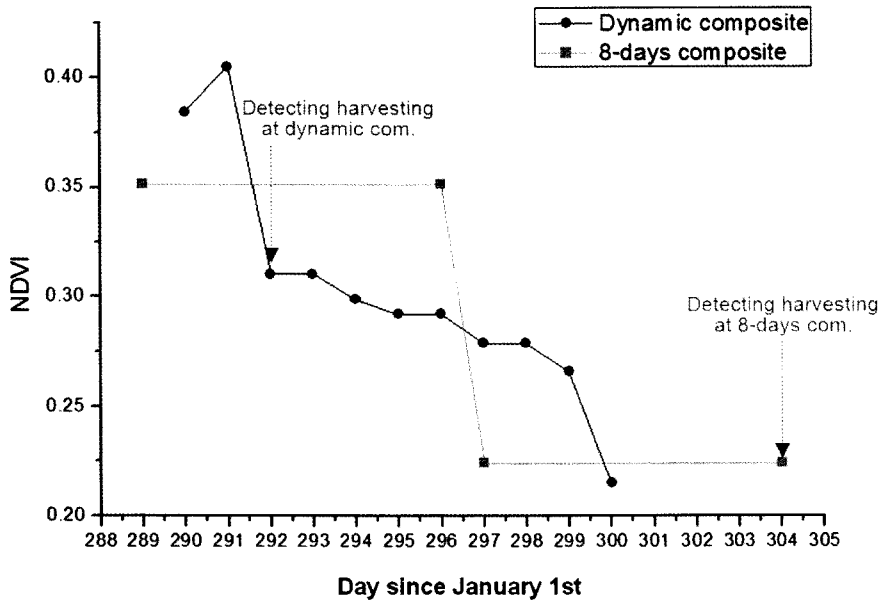

Fig. 11. NDVI temporal pattern of dynamic composite and 8-day composite dataset at harvesting area.

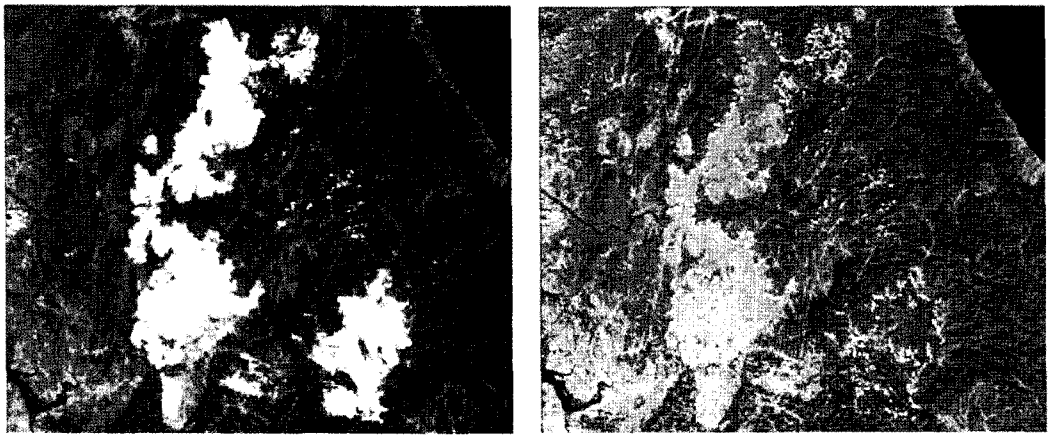

Fig. 12. Left-original MODIS color composite image(blue-MODIS band 2, green- MODIS band 3, red- MODIS band 4), right- daily dynamic composite image using October 15, 13, 12, 11(blue-MODIS band 2, green- MODIS band 3, red- MODIS band 4)

4) Future works to improve daily dynamic cloud-free composite algorithm

Daily composite image generated using daily dynamic cloud-free composite algorithm to MODIS data appears to leave vestige of the cloud area in the original MODIS data(block effect, Fig. 12). The vestige of the cloud area emerged due to the fact that pixel value differs between MODIS images acquired at different dates. In order to be effective, the daily dynamic composite method must be applied to the MODIS data that was acquired during the non-rainy season or a specific period(ex. dry season) in which many short-term changes occurred rather than being applied over one year. In the subsequent study, the spatial coherence of the dynamic composited MODIS image will be improved. Then, this composite image will be used to detect various short-term land cover changes.

4. Conclusions

The daily dynamic cloud-free composite algorithm provides daily 250 m cloud-free MODIS images. The LMVM algorithm improved the spatial resolution of the 500 m original MODIS data and generated 250 m MODIS reflective seven bands. The 250 m MODIS dataset may improve various MODIS land products such as burned area detection or classification. The dynamic daily composite algorithm showed a higher temporal resolution and provided more current information in comparison to the 8-day static composite algorithm. The dynamic daily composite algorithm detected short-term changes and improved the detection rate of the burned and harvest areas. Although the 8-day static composite MODIS showed only one standard value during the 8-day period, the dynamic composited MODIS data showed daily MODIS images and a dynamic temporal pattern. In comparison to the daily MODIS data, the dynamic composite MODIS data showed a more stable temporal pattern. This resulted because the algorithm reduced the cloud containments during the rainy season. The dynamic composite algorithm also provided the date of daily MODIS images used in compositing each pixel. This additional information accurately detected the date on which short-time changes occurred.

Our composite algorithm appears to work well in the relatively cloud-free dry season, however it may

not work well during the cloudy wet season as it is subject to the accuracy of masking cloud and shadow, the technique to mask them needs to be improved further. Cut-and-patch technique is not fully developed yet to remove "the block effect".

Acknowledgements

This research was supported by a grant (06KLSGB01) from Cutting-edge Urban Development -Korean Land Spatialization Research Project funded by Ministry of Land, transport and Maritime Affairs of Korean government.

References

Ackerman, S., K. Strabala, P. Menzel, R. Frey, C. Moeller, L. Gumley, B. Baum, S. W. Seemann, and H. Zhang, 2006. Discriminating clear-sky form cloud with MODIS, Algorithm Theoretical Basis document(MOD35), Version 5.0.

Ahl, D. E., S. T. Gower, S. N. Burrows, N. V. Shabnaov, R. B. Myneni, and Y. Knyazikhin, 2006. Monitoring spring canopy phenology of a deciduous broadleaf forest using MODIS, *Remote Sensing of Environment*, 104: 88-95.

Asner, P. A., B. H. Braswell, D. S. Schimel, and C. A. Wessman, 1998. Ecological research needs from multiangle remote sensing data, *Remote Sensing of Environment*, 63: 155-165.

Bonan, G. B., K. W. Oleson, M. Vertenstein, and S. Levis, 2003. The land surface climatology of the community land model coupled to the NCAR community climate model, *Journal of Climate*, 15: 3123-3149.

Botta, A., N. Viovy, and P. Ciais, 2000. A global prognostic scheme of leaf onset using satellite data, *Global Change Biology*, 6: 709-725.

Breaker, L. C., E. M. Armstrong, and C. A. Endris, 2010. Establishing an objective basis for image compositing in satellite oceanography, *Remote Sensing of Environment*, 114: 345-362.

Chen, J., P. Jönsson, M. Tamura, Z. Gu, B. Matsushita, and L. Eklundh, 2004. A simple method for reconstructing a high-quality NDVI time-series data set based on the Savitzky-Golay filter, *Remote Sensing of Environment*, 91: 332-344.

Chuine, I., G. Cambon, and P. Comtois, 2000. Scaling phenology from the local to the regional level: advances from species-specific phonological models, *Global Change Biology*, 6(8): 943-952.

Chuvieco, E., G. Ventura, M. P. Martin, and I. Gomez, 2005. Assessment of multitemporal compositing techniques of MODIS and AVHRR images for burned land mapping, *Remote Sensing of Environment*, 94: 450-462.

Chuvieco, E., P. Englefield, A. P. Trishchenko, and Y. Luo, 2008. Generation of long time series of burn area maps of the Boreal forest from NOAA-AVHRR composite data, *Remote Sensing of Environment*, 112: 2381-2396.

Cihlar, J., 1996. Identification of contaminated pixels in AVHRR composite images for studies of land biosphere, *Remote Sensing of Environment*, 56: 149-163.

Cihlar, J. and J. Howarth, 1994. Detection and removal of cloud contamination from AVHRR composite images, *IEEE Transactions on Geoscience and Remote Sensing*, 32: 427-437.

Cihlar, J. and F. Huang, 1994. Effect of atmospheric correction and viewing angle restriction on AVHRR composites, *International Journal of Remote Sensing*, 21: 22-27.

Cihlar, J., R. Latifovic, J. Chen, A. Trishchenko, Y.

Du, G. Fedosejevs, and B. Guindon, 2004. Systematic corrections of AVHRR image composites for temporal studies, *Remote Sensing of Environment*, 89: 217-223.

Cihlar, J., D. Manak, and N. Voisin, 1994. AVHRR bidirectional reflectances effects and compositing, *Remote Sensing of Environment*, 48: 77-88.

Cihlar, J., H. Ly, Z. Li, J. Chen, H. Pokrant, and F. Huang, 1997. Multitemporal, multichannel AVHRR data sets for land biosphere studies-artifacts and corrections, *Remote Sensing of Environment*, 60: 35-57.

de Beurs, K. M. and G. M. Henebry, 2004. Land surface phenology, climate variation, and institutional change: Analyzing agricultural land cover change in Kazakhstan, *Remote Sensing of Environment*, 89: 497-209.

Dickinson, R. E., A. Henderson-Sellers, P. J. Kennedy, and M. F. Wilson, 1986. *Biosphere-Atmosphere Transfer Scheme(BATS) for the NCAR CCM, NCAR/TN-275-STR*. Boulder, CO:NCAR Research.

Duchemin, B., D. Guyon, and J. P. Lagouarde, 1999. Potential and limits of NOAA-AVHRR temporal composite data for phenology and water stress monitoring of temperate forest ecosystems, *International Journal of Remote Sensing*, 20: 895-917.

Duchemin, B., B. Berthelot, G. Dedieu, M. Leroy, and P. Maisongrande, 2002. Normalisation of directional effects in 10-day global syntheses derived from VEGETATION/SPOT: II. Validation of an operational method on actual data sets, *Remote Sensing of Environment*, 81: 101-113.

Eidenshink, J. C., and J. L. Faundeen, 1994. The 1 km AVHRR global land data set: needs of the International Geosphere Biosphere Program, *International Journal of Remote Sensing*, 16: 3443-3462.

Fensholt, R., K. Rasmussen, T. T. Nielsen, and C. Mbow, 2009. Evaluation of earth observation based long term vegetation trends – Intercomparing NDVI time series trend analysis consistency of Sahel from AVHRR GIMMS, Terra MODIS and SPOT VGT data, *Remote Sensing of Environment*, 113: 1886-1898.

Fernández, A., P. Illera, and J. L. Casanova, 1997. Automatic mapping of surfaces affected by forest fires in Spain using AVHRR NDVI composite image data, *Remote Sensing of Environment*, 60: 153-162.

Fontana, F. M. A., A. P. Trishchenko, K. V. Khlopenkov, Y. Luo, and S. Wunderle, 2009. Impact of orthorectification and spatial sampling on maximum NDVI composite data in mountain regions, *Remote Sensing of Environment*, 113: 2701-2712.

Gallo, K., L. Ji, B. Reed, J. Eidenshink, and J. Dwyer, 2005. Multi-platform comparisons of MODIS and AVHRR normalized difference vegetation index data, *Remote Sensing of Environment*, 99: 221-231.

Gao, F., J. Masek, M. Schwaller, and F. Hall, 2006. On the blending of the Landsat and MODIS surface reflectance: Predicting daily Landsat surface reflectance, *IEEE Transactions on Geoscience and Remote Sensing*, 44: 2207-2218.

Gutman, G. and A. Ignatov, 1995. Global land monitoring from AVHRR: potential and limitations, *International Journal of Remote Sensing*, 16(13): 2301-2309.

Gutman, G. G., 1991. Vegetation indices from AVHRR: an update and future prospects, *Remote Sensing of Environment*, 35: 121-136.

Hall, F. G., J. R. Townshend, and E. T. Engmann,

1995. Status of remote sensing algorithms for estimation of land surface parameters, *Remote Sensing of Environment*, 51: 138-156.

Hall, D. K., G. A. Riggs, V. V. Salomonson, N. E. DiGirolamo, and K. J. Bayr, 2002. MODIS snow-cover products, *Remote Sensing of Environment*, 83: 181-194.

Hansen, M. C., D. P. Roy, E. Lindquist, B. Adusei, C. O. Justice, and A. Altstatt, 2008. A method for integrating MODIS and Landsat data for systematic monitoring of forest cover and change in the Congo Basin, *Remote Sensing of Environment*, 112: 2495-2513.

Hilker, T., M. A. Wulder, N. C. Coops, J. Linke, G. McDermid, J. G. Masek, E. Gao, and J. C. White, 2009. A new data fusion model for high spatial- and temporal-resolution mapping of forest disturbance based on Landsat and MODIS, *Remote Sensing of Environment*, 113: 1613-1627.

Holben, B. N., 1986. Characteristics of maximum-value composite images from temporal AVHRR data, *International Journal of Remote Sensing*, 7: 1417-1434.

Jepsen, J. U., S. B. Hagen, K. A. Høgda, R. A. Ims, S. R. Karlsen, H. Tømmervik, and N. G. Yoccoz, 2009. Monitoring the spatio-temporal dynamics of geometrid moth outbreaks in birch forest using MODIS-NDVI data, *Remote Sensing of Environment*, 113: 1939-1947.

Jin, S. and S. A. Sader, 2005. MODIS time-series imagery for forest disturbance detection and quantification of patch size effects, *Remote Sensing of Environment*, 99: 462-470.

Julien, Y. and J. A. Sobrino, 2010. Comparison of cloud-reconstruction methods for time series of composite NDVI data, *Remote Sensing of Environment*, 114: 618-625.

Kaufman, Y. J. and C. O. Justice, 1998. Algorithm Technical Background Document, MODIS Fire Products(Versions 2.2 Nov 10 1998) EOS ID#2741.

Karathanassi, V., P. Kolokousis, and S. Ioannidous, 2007. A comparison study on fusion methods using evaluation indicators, *International Journal of Remote Sensing*, 28(10): 2309-2341.

Key, C. H. and N. C. Benson, 1999. The Normalized Burned Ratio, a Landsat TM radiometric index of burn severity incorporating multi-temporal differencing.(http://nrmsc.usgs.gov/research/ndbr.htm)

Kim, S. H., 2003. Validation of MODIS Leaf Area Index product at temperate forest in Central Korea. *Master thesis*, Department of Geoinformatic Engineering, Inha University, Republic of Korea.

Kim, S. H., 2009. Development of an algorithm for detecting sub-pixel scale forest fires using MODIS data. *Ph.D. thesis*, Department of Geoinformatic Engineering, Inha University, Republic of Korea.

Kim, S. H. and K. S. Lee, 2003. Local validation of MODIS global Leaf Area Index(LAI) product over temperate forest, *Korean Journal of Remote Sensing*, 19(1): 1-9.

Kim, S.H., S. J. Kang, and K. S. Lee, 2010. Comparison of fusion methods for generating 250 m MODIS image, *Korean Journal of Remote Sensing*, 26(3): 305-316.

Latifovic, R., Z. L. Zhu, J. Cihlar, C. Giri, and I. Olthof, 2004. Land cover mapping of North and Central America-Global Land Cover 2000, *Remote Sensing of Environment*, 89: 116-127.

Le Hégarat-Mascle, S. and C. André, 2009. Use of Markov Random Fields for automatic cloud/shadow detection on high resolution

optical images, *ISPRS Journal of Photogrammetry and Remote Sensing*, 64: 351-366.

Loboda, T., K. J. O'Neal, and I. Csiszar, 2007. Regionally adaptable dNBR-based algorithm for burned area mapping from MODIS data, *Remote Sensing of Environment*, 109: 429-442.

Luo, Y., A. P. Trishchenko, and K. V. Khlopenkov, 2008. Developing clear-sky, cloud and cloud shadow mask for producing clear-sky composites at 250-meter spatial resolution for the seven MODIS land bands over Canada and North America, *Remote Sensing of Environment*, 112: 4167-4185.

Li, Z., J. Cihar, X. Zheng, L. Moreau, and H. Ly, 1996. The bidirectional effects of AVHRR measurements over boreal regions, *IEEE Transactions on Geoscience and Remote Sensing*, 34(6): 1308-1322.

Myneni, R. B., S. Hoffman, Y. Knyazikhin, J. L. Privette, J. Glassy, Y. Tian, Y. Wang, X. Song, Y. Zhang, G. R. Smith, A. Lotsch, M. Friedl, J. T. Morisette, P. Votava, R. R. Nemani, and S. W. Running, 2002. Global products of vegetation leaf area and fraction absorbed PAR from year one of MODIS data, *Remote Sensing of Environment*, 83: 214-231.

Pinzon, J., M. E. Brown, and C. J. Tucker, 2005. EMD correction of orbital drift artifacts in satellite data stream. In N. Huang and S. Shen(Eds.), *The Hilbert-Huang transform and its applications*(pp. 167-183). Hackensack NJ: World Scientific Publishing Co.

Potter, C., S. Kloster, V. Genovese, and R. B. Mymeni, 2003. Satellite data help predict terrestrial carbon sinks, *EOS*, 84(46): 502-508.

Potapov, P., M. C. Hansen, S. V. Stehman, T. R. Loveland, and K. Pittman, 2008. Combining MODIS and Landsat imagery to estimate and map boreal forest cover loss, *Remote Sensing of Environment*, 112: 3708-3719.

Robertson, D. M., R. A. Ragotzkie, and J. J. Magnuson, 1992. Lake ice records used to detect historical and future climatic changes, *Climatic Change*, 21(4): 407-427.

El Saleous, N. Z., E. F. Vermote, C. O. Justice, J. R. G. Townshend, C. J. Tucker, and S. N. Goward, 2000. Improvements in the global biospheric record from the advanced very high resolution radiometer, *International Journal of Remote Sensing*, 21: 1251-1278.

Simpson, J. J. and J. R. Stitt, 1998. A procedure for the detection and removal of cloud shadow from AVHRR data over land, *IEEE Transactions on Geoscience and Remote Sensing*, 65: 1-24.

Stroeve, J., J. E. Bax, F. Gao, S. Liang, A. Nolin, and C. Schaaf, 2005. Accuracy assessment of the MODIS 16-day albedo product for snow: comparisons with Greenland in situ measurements, *Remote Sensing of Environment*, 94: 46-60.

Stroppiana, D., S. Pinnock, J. M. C. Pereira, and J. M. Grégoire, 2002. Radiometric analysis of SPOT-VEGETATION images for burnt area detection in Northern Australia, *Remote Sensing of Environment*, 82: 21-37.

Tian, Y., R. E. Dickinson, L. Zhou, X. Zeng, Y. Kai, R. B. Myneni, Y. Knyazikhin, X. Zhang, M. Friedl, H. Yu, W. Wu, and M. Shaikh, 2004. Comparison of seasonal and spatial variations of leaf area index and fraction of absorbed photosynthetically active radiation from Moderate Resolution Imaging Spectroradiometer (MODIS) and Common Land Model, *Journal of Geophysical Research*, 109(D01):103.doi: 10.1029/2003JD003777.

Tucker, C. J., J. E. Pinzon, M. E. Brown, D. A. Slayback, E. W. Pak, R. Mahoney, E. F. Vermote, and N. E. Saleous, 2005. An

extended AVHRR 8-km NDVI dataset compatible with MODIS and SPOT vegetation NDVI data, *International Journal of Remote Sensing*, 26: 4485-4498.

White, M. A. and R. R. Nemani, 2006. Real-time monitoring and short-term forecasting of land surface phenology, *Remote Sensing of Environment*, 104: 43-49.

Yang, W., N. V. Shabanov, D. Huang, W. Wang, R. E. Dickinson, R. R. Nemani, Y. Knyazikhin, and R. B. Myneni, 2006. Analysis of leaf area index products from combination of MODIS Terra and Aqua data, *Remote Sensing of Environment*, 104: 297-312.